PROGRESS IN PHOTOVOLTAICS: RESEARCH AND APPLICATIONS
Prog. Photovolt: Res. Appl. 2016; **24**:1346–1358
Published online 22 June 2016 in Wiley Online Library (wileyonlinelibrary.com). DOI: 10.1002/pip.2793

RESEARCH ARTICLE

Changes of solar cell parameters during damp-heat exposure

Jiang Zhu[1]*, Michael Koehl[2], Stephan Hoffmann[2], Karl Anton Berger[3], Shokufeh Zamini[3], Ian Bennett[4], Eric Gerritsen[5], Philippe Malbranche[5], Paola Pugliatti[6], Agnese Di Stefano[6], Francesco Aleo[6], Dario Bertani[7], Fabrizio Paletta[7], Francesco Roca[8], Giorgio Graditi[8], Michele Pellegrino[8], Oihana Zubillaga[9], F. J. Cano Iranzo[9], Alberto Pozza[10], Tony Sample[10] and Ralph Gottschalg[1]

[1] Centre for Renewable Energy Systems Technology (CREST), Wolfson School of Mechanical, Electrical and Manufacturing Engineering, Loughborough University, Leicestershire, LE11 3TU, UK
[2] Fraunhofer ISE, Freiburg im Breisgau, Germany
[3] Energy Department of the Austrian Institute of Technology (AIT), Vienna, Austria
[4] ECN, Petten, The Netherlands
[5] CEA-INES, Le Bourget-du-Lac, France
[6] ENEL, Rome, Italy
[7] RSE, Milan, Italy
[8] ENEA, Rome, Italy
[9] TECNALIA Research and Innovation, San Sebastian, Spain
[10] European Commission, DG Joint Research Centre, Ispra, Italy

ABSTRACT

The electrical ageing of photovoltaic modules during extended damp-heat tests at different stress levels is investigated for three types of crystalline silicon photovoltaic modules with different backsheets, encapsulants and cell types. Deploying different stress levels allows determination of an equivalent stress dose function, which is a first step towards a lifetime prediction of devices. The derived humidity dose is used to characterise the degradation of power as well as that of the solar cell's equivalent circuit parameters calculated from measured current–voltage characteristics. An application of this to the samples demonstrates different modes in the degradation and thus enables better understanding of the module's underlying ageing mechanisms. The analysis of changes in the solar cell equivalent circuit parameters identified the primary contributors to the power degradation and distinguished the potential ageing mechanism for each types of module investigated in this paper. © 2016 The Authors. *Progress in Photovoltaics: Research and Applications* published by John Wiley & Sons Ltd.

KEYWORDS

solar cells; photovoltaic modules; damp-heat; ageing; degradation; modelling

***Correspondence**

Jiang Zhu, Centre for Renewable Energy Systems Technology (CREST), Wolfson School of Mechanical, Electrical and Manufacturing Engineering, Loughborough University, Leicestershire LE11 3TU, UK.
E-mail: J.Zhu@lboro.ac.uk

Received 25 May 2015; Revised 21 April 2016; Accepted 17 May 2016

1. INTRODUCTION

The durability of photovoltaic (PV) modules is a key factor for the financial viability of an installation and potentially the main distinction between different types of PV modules. However, the link to operating conditions remains to be established as discussed, for example, in [1]. This requires further work on understanding on the stress factors as well as the response of the PV modules to different environments. The latter is to be addressed in this work, where the ageing of modules is investigated at static damp-heat (DH) conditions at various conditions of temperature and

humidity in order to generate the understanding that is required to predict longevity in the real environment.

A series of (non-standard) accelerated ageing tests have been carried out within the European Photovoltaic Research Infrastructure project SOPHIA including DH, thermal cycling, UV, mechanical load and combinations of these, in order to explore different ageing mechanisms and develop a modelling approach for the observed degradation. Current–voltage (I-V), electroluminescence (EL) and insulation measurements were carried out to characterise ageing mechanisms [2–5]. This paper focusses exclusively on DH-induced ageing observed for three different types of crystalline silicon PV modules.

Various indoor stress tests are used in the industry to investigate PV module reliability and certify designs. These may help in understanding the degradation mechanisms in the field. They do not, however, predict the module lifetime in real outdoor operation, despite this being one of the assumptions often made. In testing the humidity resistance of modules, typically, the DH test specified in IEC 61215 [6] is used. This qualification test specifies the DH test to be 1000 h at 85°C and 85% relative humidity (RH). These tests are useful to identify design, material and manufacturing issues that may lead to premature failures in the field [1],[7–9]. Unfortunately, these tests can only give a pass/fail criterion but do not give any information on the durability of modules. The latter requires a link to variable environmental conditions. A first step towards linking module degradation to environmental stresses is the stress testing in static conditions at a number of stress levels as being done in this paper.

Damp-heat tests impose a high amount of water vapour on the surface of PV modules and drives this into the module. The process of water vapour permeation is accelerated by elevated temperatures. This leads to various degradations such as corrosion, delamination or discoloration [10–14]. Corrosion is a major aspect of module ageing, which is typically caused by chemical, physical or electrochemical reactions, for example, corrosion of cells, anti-reflection coating, solder bonds and silver fingers. For ethylene-vinyl acetate (EVA)-encapsulated modules, acetic acid is a by-product produced by the hydrolysis reaction during DH test, and the accumulation of the generated acetic acid within the module will lead to chemical corrosion of electrodes [15] and accelerate the metallization corrosion [16–18]. This is one of the most important degradation factors for EVA encapsulated PV modules. EVA also undergoes thermal degradation at temperature above 300°C, at which condition the EVA becomes instable and the acetic acid is evolved as a main product [19]. This temperature range is out of the testing condition; therefore, its impact is not considered in the current degradation analysis. Because of the effect of water ingress, delamination of backsheet or encapsulant is another degradation mechanism widely observed in the field [20,21]. The magnitude of the DH stress has been shown to result in significant differences in the delamination, as investigated in [22]. The delamination failures might occur at interface between glass and EVA or between EVA and backsheet, and the failure interface could also alter during ageing. This gives a further indication that the static 85°C/85%RH test may not give the required answers during a testing cycle.

Most of the work mentioned earlier reported on the degradations of device maximum power or measurable chemical and mechanical properties of materials. It has been shown that there are difficulties in developing an appropriate testing protocol to investigate long-term degradation mechanisms and examine module durability. In this paper, analysis focuses on the solar cell equivalent circuit parameters in an attempt to extract useful information on the degradation mechanisms and identify the key contributors and failure modes at module level during the different stages of DH ageing. Some previous study on degradation of the equivalent circuit parameters can be found [23,24]. These cover degradation in general but not really the detailed analysis of the activation energies as done here. The work presented is to develop the link between environmental stresses, material properties of the encapsulation and device performance. The analysis of equivalent circuit parameters can be seen as an intermediate step allowing an estimation of the underlying degradation mechanism. This allows a better insight than the commonly used analysis of power values. Furthermore, it allows a link to energy production, which is not really possible when using power values as devices with the same power degradation may have very different energy yields (see, e.g. [25] for an explanation of this). An objective is to see if different DH conditions trigger different degradation mechanisms and thus to verify the validity of the stress conditions currently being applied. The solar cell equivalent circuit parameters are calculated from the measured I-V curves during module ageing and thus the changes in these parameters can be observed.

The overall aim is to enable lifetime (energy) prediction from failure modes seen due to DH stresses. The assumption is that these can be simulated with steady state conditions, and an equivalent dose for the ageing can be used. The paper reports on the developed testing protocol, that is, DH tests at different temperature and RH conditions. The results for a number of crystalline silicon modules are given, and the ageing is analysed for demonstrating the applicability of the approach. Devices I-V were measured regularly as well as the EL. Equivalent circuit solar cell parameters are extracted from the I-V measurements, and their changes with time are discussed in the context of the EL images. The degradations of different parameters are then analysed in terms of a derived humidity dose. The dose used here is a stress function that considers temperature as an accelerant (rather than a stress) and assumes an activation energy for better description. Its derivation is given in Section 2.4. The key module's equivalent circuit parameter contributing to the power degradation can be identified, and some conclusions with respect to the primary ageing mechanism can be drawn. A major advantage of the approach is, for example, that one can verify that the correct mechanism is accelerated in the process, as otherwise higher temperature ageing could not be mapped with

DOI: 10.1002/pip

the same dose function. In the given example, some parameters may start to degrade a few hundred hours earlier than other parameters, which indicates different ageing mechanisms in the modules tested or at least different stages of the same mechanism (e.g. induction, ageing and stabilisation). Different primary equivalent circuit parameters are identified for different types of modules, which indicate different failure modes. This is almost certainly because of module design, materials used or manufacturing process.

2. ACCELERATED AGEING TESTS AND MEASUREMENTS

2.1. Ageing test and measurements plan

A distributed DH stress test of three types of PV modules has been carried out at five conditions for extended times. Tests have been carried out at 85°C/85%RH, 75°C/85% RH, 95°C/85%RH, 95°C/70%RH and 90°C/50%RH under the framework of the SOPHIA project at different test laboratories for up to 6500 h. Three types of PV modules from three manufacturers (Type A, Type B and Type C) with different types of cells, encapsulants and backsheets were used in the tests. There were two types of cells (p-type homojunction c-Si cell and n-type heterojunction c-Si cell), two types of encapsulant, that is, conventional EVA (properly cured EVA is a plastic material) and a silicone-based thermoplastic material, and different backsheets with one having an aluminium layer as additional moisture barrier. Table I indicates the different materials for the three module types used in the tests.

For each DH condition, two samples of each module type were tested. Thus, there were 10 samples of each module type, that is, A1-10, B1-10 and C1-10. Each test thus included six modules, that is, two modules from each of the three types. Table II summarises the DH exposures and characterisation measurements schedule for one module type with module numbers, testing temperature and RH levels, total durations and the measurement time intervals. The I-V curve and EL image were taken periodically for each module during the course of test to monitor the progression of ageing. The I-V curves, which were also used for extracting solar cell equivalent circuit parameters for ageing mechanism analysis, were measured at various systems and corrected to Standard Testing Conditions. The laboratories also participated in a round robin intercomparison [26] to ensure comparability of the measurements. The EL images were taken with the injected current equals to module's I_{SC}.

2.2. Degradation of maximum power

This section reports the degradation in the power at maximum power point (P_{MPP}) against ageing time for all tested samples of each module type.

Figure 1(a)–(c) plots the normalised P_{MPP} in dependence of DH level of module Type A, B and C. All three types of modules have passed the IEC standard test, that is, 1000 h of DH at 85°C/85%RH (refer to A5-6, B5-6 and C5-6). All modules showed only minor degradation in power, but there was a significant differentiation in the extended tests. Module Type A with EVA encapsulant and normal backsheet showed the largest degradation (Figure 1a) for all DH levels comparing with Type B and C. The four modules aged at 95°C (A1-2 and A7-8) showed the fastest degradation. There typically are three distinct phases in the ageing process, which are represented by an 'S'-shape in the curve. There is an initial induction phase, the actual (rapid) degradation phase and a levelling out or stabilisation. The latter occurs when the specific degradation mechanism being triggered by the environmental stresses has done close to its maximum damage and further degradation of this parameter will not significantly affect performance. Modules A1-2 and A7-8 lost about 70% of their initial power in the stress tests. This clearly is outside typical warranty conditions but can be attributed to overstressing, that is, applying stresses in excess of what is normally been seen in the field. Power degradation for realistic exposure was reported to be on average below 20% after being fielded for 20 years [20]. The modules aged at lower temperature and relative humidity levels (A3-4, A5-6 and A9-10) showed slower degradation levels. They started the rapid degradation phase after 3000–5000 h ageing, a few thousand hours later than those at 95°C (A1-2 and A7-8). They did not reach stabilisation before the end of these tests.

Module Type B (Figure 1b) has an aluminium moisture barrier in backsheet, which prevented the moisture ingress by diffusion through the backsheet during the tests. The modules B3-4 and B5-6 aged at 75–85°C showed minor degradation after extended tests, that is, they were still in the induction phase. Only the modules B1-2 and B7-8 at 95°C started to degrade after around 3000 h, whereas the

Table I. Photovoltaic modules used for damp-heat tests.

Manufacturer	Type of cell	Type of encapsulant	Backsheet with aluminium moisture barrier
A	P-type homojunction	Plastic: EVA	No
B	N-type heterojunction	Plastic: EVA	Yes
C	P-type homojunction	Thermoplastic: silicone	No

EVA, ethylene-vinyl acetate.

2016; **24**:1346–1358
DOI: 10.1002/pip

Table II. Summary of damp-heat testing plan.

Module No.	T (°C)	RH (%)	Duration (hours)	Measurement intervals (hours)
1, 2	95	70	4250	0, 1000, 1250, 1500, 1750, 2000, 2250, 2500, 2750, 3000, 3250, 3750, 4250
3, 4	75	85	6500	0, 2000, 4000, 5000, 5500, 6000, 6500
5, 6	85	85	4000	0, 500, 1000, 1500, 2000, 2500, 3000, 3500, 4000
7, 8	95	85	3000	0, 600, 1000, 1500, 2000, 2060, 2500, 3000
9, 10	90	50	4000	0, 1000, 1250, 1500, 1750, 2000, 2250, 2500, 2750, 3000, 3250, 3500, 4000

modules B9-10 at 90°C appeared to degrade after about 4000 h.

Module Type C (Figure 1c) uses a silicone-based thermoplastic material as encapsulant and thus there is no generation of acetic acid attacking the solar cells and metal contacts. Modules showed stable behaviours in most cases except for the modules C1 and C2, which were degraded under 95°C/70%RH and lost structural integrity. The two modules had early failures due to the melting of the thermoplastic material that leads to the solar cells sliding in the module and damages to the cells and circuits (Figure 2).

2.3. Electroluminescence images

The EL images were taken for all modules during the course of the extended DH tests with the injected current equals to module's short-circuit current. Analysing the evolution of the images may identify specific degradation mechanisms.

Figure 3 shows the EL image evolution for one typically degraded module of each type. Different degradation patterns can be observed in the EL images. The EL images of module Type A (Figure 3a) showed a typical degradation pattern due to DH ageing that is also observed elsewhere, for example, [27]. The dark area around the outside of each individual cell indicates reduced radiant recombination at the periphery of each cell. This points to humidity ingression through the backsheet and diffusing through the material around the cell. This creates a spatially graded hydrolysis of the EVA, that is, higher levels in between the cells and then expanding over the cells where humidity has a longer way to travel. Thus, a spatial variation is apparent. The degradation will occur due to a number of degradation mechanisms. The behaviour observed can be explained by three separate stages of degradation:

(1) Creation of shunting paths around the edges of the cell, potentially by increased conductivity of the encapsulant. This is seen from the increased slope around I_{SC} shown in Figure 7.
(2) A potential loss in surface passivation, that is, an increase in non-radiative surface recombination [28]. This explains the observed darkening of the image at cell edges. This will in turn result in highly localised degradation. Typically, the voltage would initially not be affected by this as in the case of inhomogeneous voltage across different parts of the cell localised voltage drops are masked (see, e.g. [29,30] for explanations). With progressing deterioration, the collection of current will be affected significantly, which will result in the reduction of currents.
(3) In the final stages, corrosion of the cell contacts due to the interaction with the acetic acid generated will result in an increase of series resistance [16–18]. This is apparent from the increase in the slope at V_{OC} at the later stages of degradation.

Module Type B (Figure 3b) showed a different pathway of moisture ingress. Its backsheet was a better moisture barrier, which significantly reduced the rate of humidity ingress. A dark area was observed starting from the periphery of the module and the area around the junction box. The absolute brightness of the measurement is strongly dependent on the measurement conditions, but the relative brightness between adjacent cells became more obvious after ageing, which may indicate different cells ageing slightly differently.

There was no obvious change in EL images of Module Type C (Figure 3c) except for the ones that suffered early failures of the encapsulant losing structural integrity (as shown in Figure 2). This relative stable behaviour of these devices overall is due to the different encapsulant used by the module C (silicone based) rather than the conventional EVA used by the modules A and B. Although the moisture diffusivity of silicone is higher than that of EVA [31], silicones have no mechanism for generating ionic material in the presence of moisture, whereas the EVA uses peroxide catalysts that might produce acidic by-products attacking cells. However, at elevated temperature (95°C), the thermoplastic material lost its structural integrity and failed due to the cells slide damaging the circuit.

2.4. Correlation of power degradation

The underlying assumption is that the degradation mode is the same in all modules of each type. The clustering with RH and the spacing with temperature in Figure 1 gives an indication that temperature is an accelerant while the active stress is RH. A dose model has been developed by Koehl *et al.* [32] and is used here to analyse the results further. A dose represents the amount of stress imposed on a PV module during the ageing test. A dose function *dose (t)* for DH stress can be expressed as

DOI: 10.1002/pip

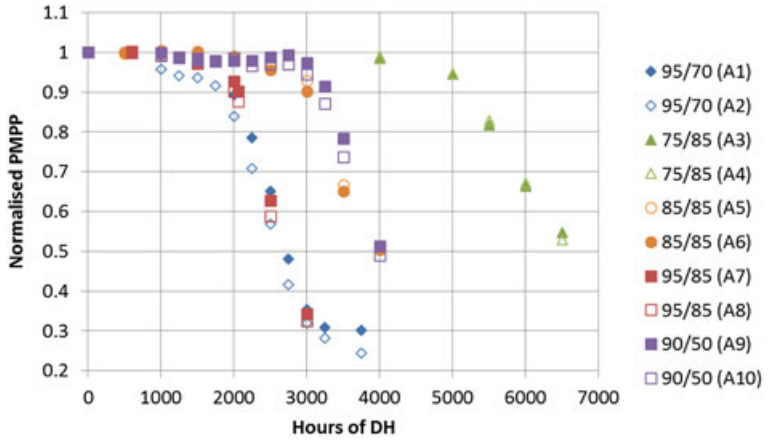

(a)

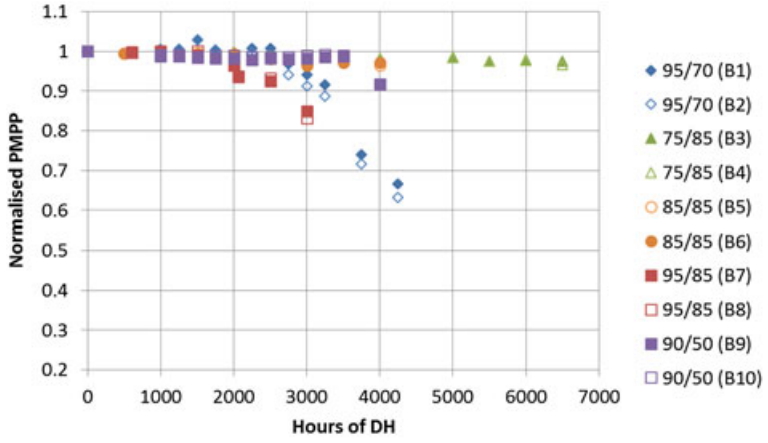

(b)

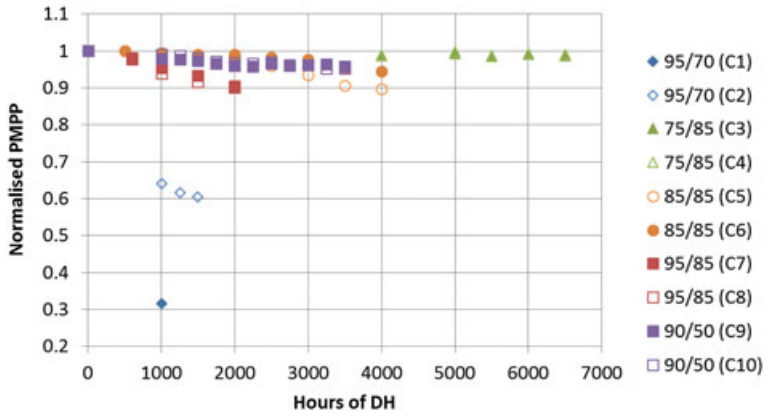

(c)

Figure 1. Degradation of power at maximum power point (P_{MPP}) over ageing time in dependence of damp-heat (DH) conditions for the three types of modules (a) Type A, (b) Type B and (c) Type C.

$$dose(t) = f\left(E_a, RH_{eff}, T, t\right) = RH_{eff}{}^{n} * e^{-\frac{E_a}{RT}} * t \quad (1)$$

where E_a is the activation energy, RH_{eff} is the effective relative humidity [32] and n is a scaling factor determining the weight of humidity effect on ageing. The scaling factor is purely empirical. It has been determined in this study by numerical fitting. It was found that the value of $n = 0.35$ gives an excellent agreement, and this value is used in the following.

2016; **24**:1346–1358
DOI: 10.1002/pip

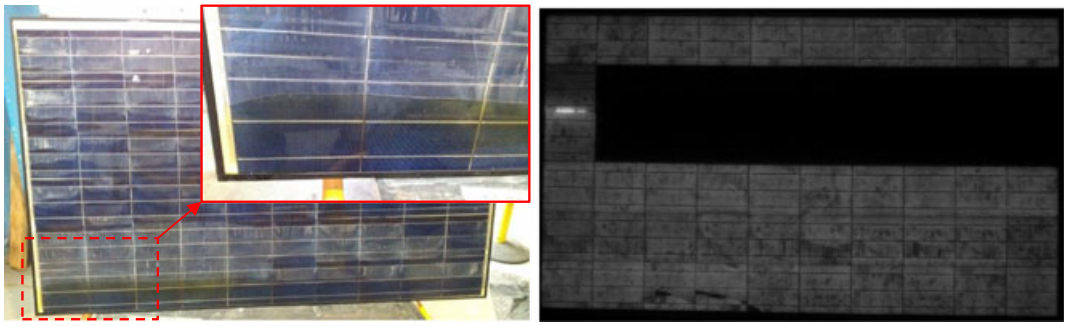

Figure 2. Visual and electroluminescence images of the module C2 suffering the early failure due to loss of structural integrity. Encapsulant lost structural integrity and strings of cells slid down causing circuit damages.

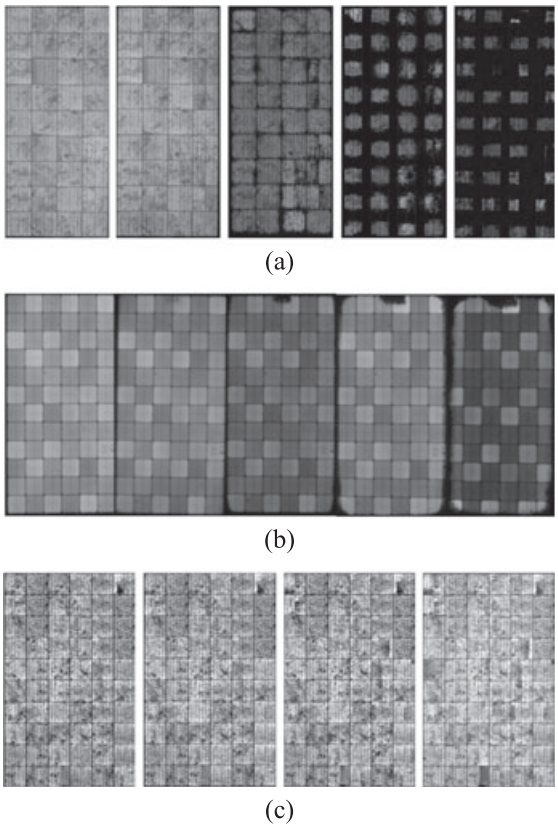

Figure 3. Evolution of electroluminescence images during the course of damp-heat tests for the three types of modules (a) Type A under 95°C/70%RH, (b) Type B under 95°C/70%RH and (c) Type C under 85°C/85%RH.

R is the gas constant and t is the testing time. The purpose of using this dose function is to quantify and evaluate the stress level, for example, DH stress level in this work at various temperature and humidity conditions, and thus it allows for comparison study of module degradation behaviours for the modules undergone ageing tests at multiple DH conditions.

The power degradation of the module Type A is used to demonstrate the applicability of this methodology. The dose model was applied to the degradation of P_{MPP} for all tested modules as shown in Figure 1a. By analysing the degradation rates ($R_d = 1/MTTF$, Mean Time To Failure, which is defined as the time when the module degrades by 20% of its initial power) for modules at the same humidity and different temperatures, that is, 75°C/85%RH, 85°C/85%RH and 95°C/85%RH, the E_a can be obtained by plotting $\ln(R_d)$ against 1/T (as shown in Figure 4), where $-E_a/R$ is equal to the slope of the trend line. As relative values only are required in determining the E_a, the relative unit of measurement, that is, procedure defined unit (p.d.u.) is used for R_d. For the module Type A, the calculated E_a is 49 kJ/mol.

The degradation in P_{MPP} observed in the different exposure tests can then be plotted against the dose as shown in Figure 5a. All modules follow a similar power degradation curve. The ageing behaviour can be modelled by a modified sigmoid function (e.g. $1 + S/(1 + exp(dose\text{-}t)$, S and t are variables fitted from measured data). This is indicated by the solid lines in Figure 5. The unit of the dose function is a relative unit showing the amount of stress and thus procedure defined unit (p.d.u.) is labelled in all dose-related figures. It can be calculated that, for the A type modules, one unit of dose as shown in Figure 5a is equivalent to 1430 h DH stress at 85°C/85%RH.

Similarly, the E_a for the module Type B can be obtained, which is 62 kJ/mol. The degradation of P_{MPP} versus the calculated dose is plotted in Figure 5b. All modules follow a same degradation curve. Because of the limitation of data points for module Type B, only the first and second phases of DH ageing can be observed at the moment.

As all modules of the Type C except the early failed ones degraded less than 10% of their initial power, the dose function for module Type C cannot be established.

Comparing the degradation curves of module Type A and B, the A modules requires a lower dose of stress than the B modules does to trigger the power degradation.

DOI: 10.1002/pip

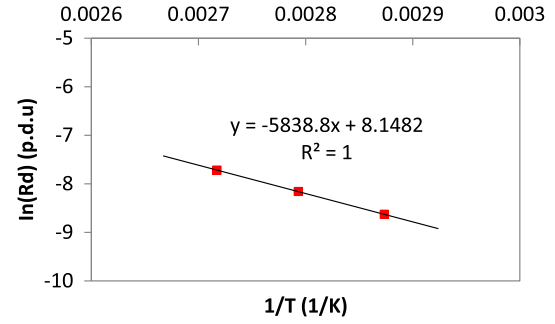

Figure 4. Calculation of activation energy (E_a) for the dose function. RH = 85%.

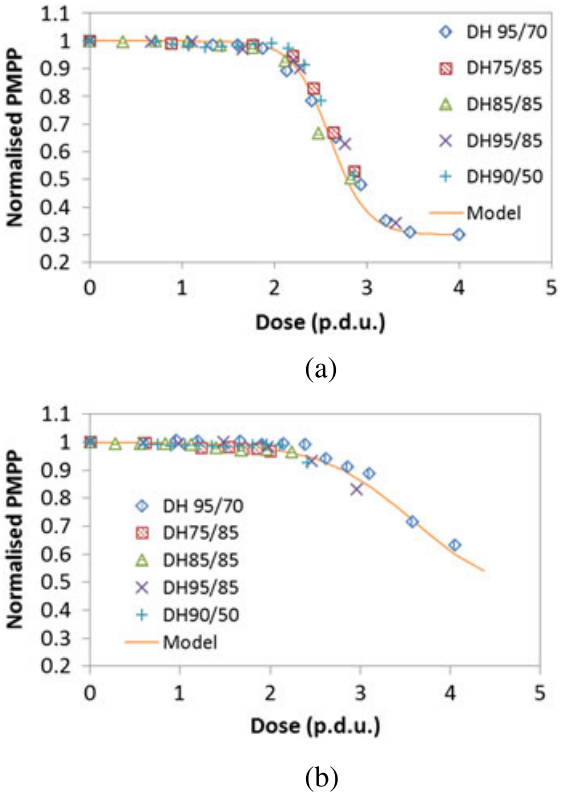

Figure 5. Degradation of maximum power (P_{MPP}) versus humidity dose in dependence of damp-heat (DH) conditions for two types of the tested modules (a) Type A and (b) Type B. Solid lines indicate the modelling degradation curves.

2.5. Correlations of short-circuit current, open-circuit voltage and fill factor degradations

With the same dose functions derived in the last section for P_{MPP}, the degradations of short-circuit current (I_{SC}), open-circuit voltage (V_{OC}) and fill factor (FF) can be analysed for Module Type A and Module Type B, respectively. As depicted in Figure 6a, the Type A modules saw degradations in both I_{SC} and FF. The V_{OC} did not show obvious degradation. The Type B modules, as depicted in Figure 6b, showed degradation in FF only. No or minor degradation in I_{SC} and V_{OC} was observed.

The dose analysis for I_{SC}, V_{OC} and FF reveals that the two types of modules underwent different ageing. The power degradation was caused by losses in I_{SC} and FF for Type A modules, whereas for Type B modules the power degradation was caused by FF reduction alone. Although the loss in FF played an important role for both types of modules, the underlying failure mechanisms are different, which can be identified by investigation of module's I-V characteristics and solar cell equivalent circuit parameters.

3. SOLAR CELL EQUIVALENT CIRCUIT PARAMETERS

The equivalent circuit of a PV module describes the device on the basis of more physical parameters such as series resistance or shunt resistance of the cells and thus allows an insight into the underlying failure mechanisms. Module Type C did not show much degradation during the DH tests and thus only the modules Type A and B are investigated in this section.

3.1. I-V characteristics

The I-V curves were measured periodically during the course of the DH tests for all tested modules. The changes in the shape of I-V curves observed are presented in Figure 7.

Figure 7 plots the I-V curves measured at different stages of ageing for two Type A modules (A1 and A3) and two Type B modules (B1 and B9). For each module type, the two modules showed similar degradation behaviours in the I-V evolution, although they were aged under different DH conditions, indicating that the underlying failure modes are similar.

Type A modules, as depicted in Figure 7a, have the degradation initially manifested in a reduction of the FF, potentially because of a decrease in slope around Voc, that is, a slight increase of series resistance. This was followed by significant reduction in the I_{SC}. Its V_{OC} remained unchanged.

Type B modules follow a significantly different pattern, despite having about the same power degradation when fully degraded. This would indicate that the degradation mechanism is fundamentally different in this case. This is shown in Figure 7b. The degradation was initiated and driven by the reduction in FF only, while its I_{SC} and V_{OC} remained stable. The main difference in the FF change here is also the very noticeable change in the slope around Isc, which is dominating the FF decrease. This indicates the underlying ageing is very different as this particular slope is an indication of shunting within the device or the cell being less homogeneous

2016; **24**:1346–1358
DOI: 10.1002/pip

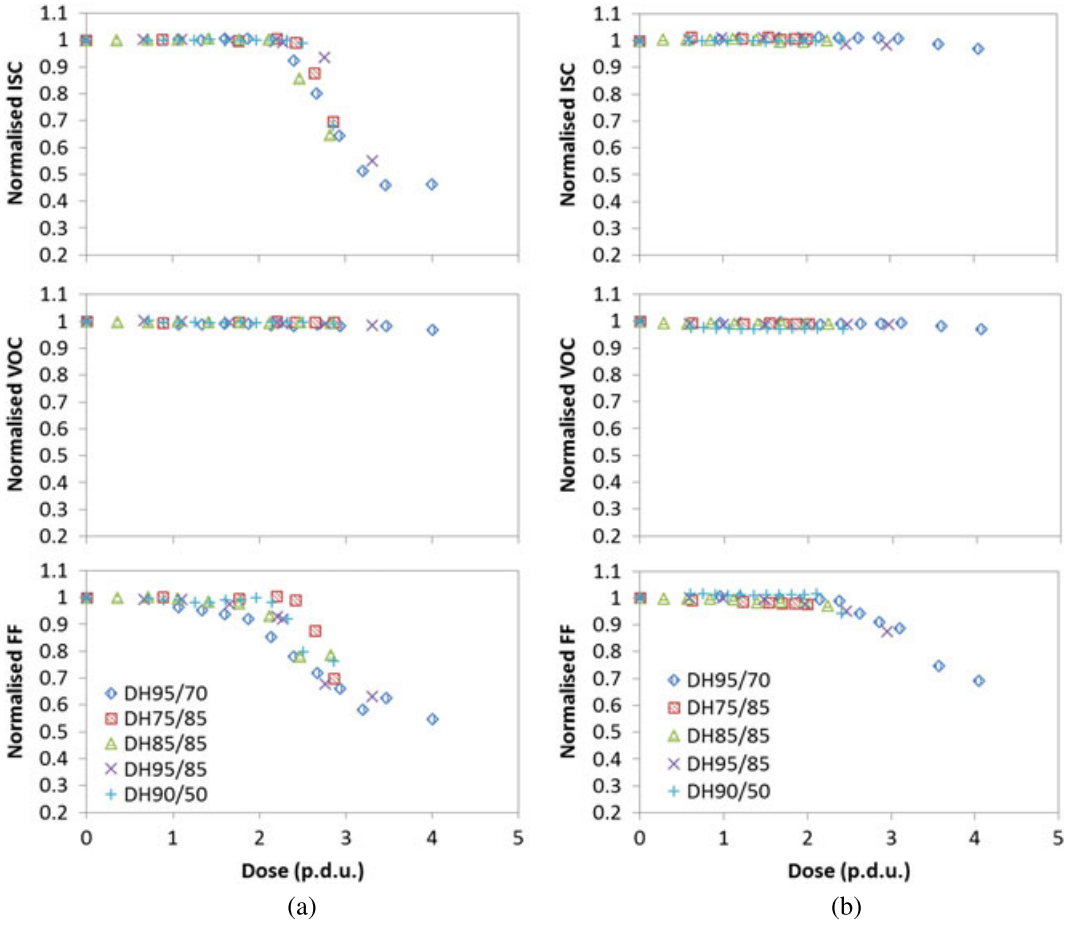

Figure 6. Degradation of short-circuit current (I_{SC}), open-circuit voltage (V_{OC}) and fill factor versus humidity dose in dependence of damp-heat (DH) conditions for (a) Module Type A and (b) Module Type B.

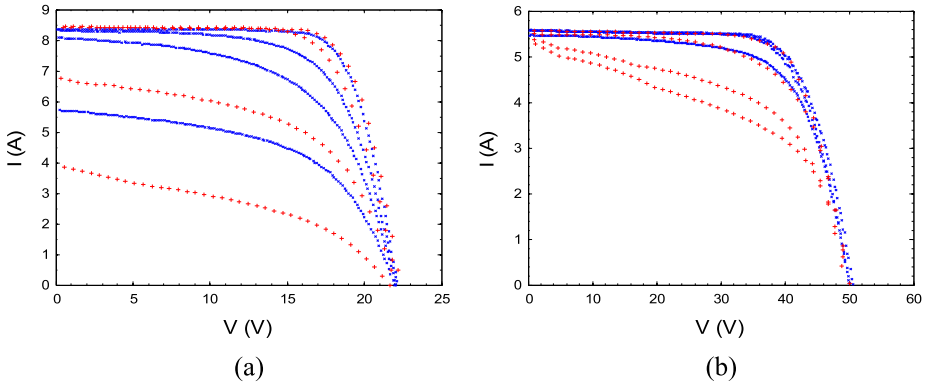

Figure 7. Evolution of current–voltage (I-V) characteristics of (a) A1 (red markers) and A3 (blue markers) and (b) B1 (red markers) and B9 (blue markers) during the course of the damp-heat tests. The modules were degraded under different temperature and relative humidity levels, but have shown similar degradation behaviours in I-Vs.

[29]. This is increasing during the test. This would be supported by the degradation in the EL images being observed initially at the junction box. Overall, degradation is distinctly different to Type A modules.

In order to quantify these issues observed by eye and potentially separate the two effects, the module's equivalent circuit parameters for the two types of modules were analysed.

DOI: 10.1002/pip

3.2. Estimates of solar cell equivalent circuit parameters

A modified double-diode model is used to represent PV module's[1] equivalent circuit parameters of which can be extracted from measured I-V characteristics. There are a number of extraction methods, for example, [33–37]. The optimum extraction is normally assessed by the quality of re-built I-V curves. It is influenced by not only the factors such as initial estimations of parameters, optimization algorithms and error criteria, but also by the extraction method as discussed in [38]. As the modules were tested and measured in five research laboratories across Europe, the measurement condition, that is, number of measurement points for each I-V, measurement error and stability and so on., would not be the same. Thus there was no optimum extraction method for all measurement data from different laboratories. However, the purpose of this work is to track the relative changes in solar cell parameters during the course of device ageing, which focuses on the relative value rather than the absolute value of each parameter. It has been tested by the authors that the relative changes in the solar cell parameters investigated in this paper are not influenced by the usage of different extraction methods. The optimum extraction of solar cell parameters is not the interest of this paper and will not be discussed further.

More importantly, the extraction is based on the assumption that the cells in the module are identical, which is unlikely to be the case. In the case of inhomogeneous devices, the losses due to shunting will be underestimated as mismatch tends to cause an increase in the FF and increase in apparent R_p. An indication of this being the case is the rather high diode ideality factor. Thus, the values calculated here give trends for the average module parameter but should not be taken as quantitative, physical parameters.

3.3. Changes of solar cell equivalent circuit parameters

The A and B type modules were used for this study. The solar cell equivalent circuit parameters, including photocurrent (I_{ph}), series resistance (R_s), parallel resistance (R_p), diode recombination current (I_{r0}) and diode ideality factor (n), were extracted from I-V curves measured at Standard Testing Conditions [33] over the course of ageing for the modules that were aged under different temperature and humidity levels. The degradation behaviours of each parameter are plotted versus the derived humidity dose as shown in Figure 8.

[1]The assumption is that all parameters of the cells are identical and a 'mixed' equivalent circuit parameter is extracted from the I-V. This clearly is an oversimplification but the best one can do with one I-V curve for the module alone without destructive testing. Especially parallel resistance, diode ideality factor and saturation current will be affected by this.

Each parameter of module Type A or Type B appeared to follow a similar degradation trend, respectively, regardless of the modules being aged under different conditions. This confirms again that all modules of each type experienced the same degradation modes under these DH conditions. The changes were triggered when the dose of stress reached certain level and stopped once the dominant ageing process has done its maximum damage (i.e. has reached the self-limitation). Comparing the same parameter, the two module types showed similar degradation patterns in I_{r0} and n, but different degradation trends in I_{ph}, R_s and R_p. Hence, two module types saw different degradation modes due to DH stresses and the impacts of the changes of solar cell equivalent circuit parameters are discussed in the succeeding text.

The I_{r0} and n of module Type A started to change earlier than other parameters did. The global n changed from 1.5 to 7, while the V_{OC} remained unchanged. This is attributed to the cell's ageing inhomogeneously, and the unphysically high value of the diode ideality factor is due to cell mismatch. This indicates that the degradation in power of the module Type A was initiated by the cell mismatch effect, which caused the losses in FF as seen from Figure 6a. However, this was a secondary effect, and its I_{ph} and R_s appeared to change as modules received more dose of stress (around dose = 2.5), at which level the P_{MPP}, I_{SC} and FF started to degrade rapidly. This reveals that the main cause to the power degradation of the A type modules is the loss in I_{ph}, which led to I_{SC} reduction, and the increase in R_s that caused further FF loss. Corrosions of the electrical circuit, for example, busbars, fingers, cell interconnects, contacts and so on, are the primary reason for R_s increase [15,39]. The loss of I_{SC} is correlated to the EL images (as shown in Figure 3a) as the cell active area became smaller.

Type B modules had similar changes in I_{r0} and n as the Type A modules did. However, they did not see degradations in I_{ph} or R_s, which maintained almost unchanged until the end of the tests. This explains that there was no reduction observed in I_{SC} (as shown in Figure 6b and 7b). The biggest difference between the two module types is seen as the different change patterns in R_p, where type A modules had a decreased R_p and type B modules saw an increased R_p during the ageing process. Normally, R_p would decrease during module degradation as an indication of shunting. However, an increased R_p that was extracted from the global module I-V characteristics can be explained by the inhomogeneous degradations across the module. Each cell in a module degraded at different rates and the module overall performance is normally limited by the cell having the largest degradation. Thus, the slightly mismatched cells may lead to the increase in the extracted global R_p [29]. Meanwhile, the module global ideality factor n increased from 2 to 5 as shown in Figure 8b, which also indicates the cell mismatch effect. Furthermore, the identification of

2016; **24**:1346–1358
DOI: 10.1002/pip

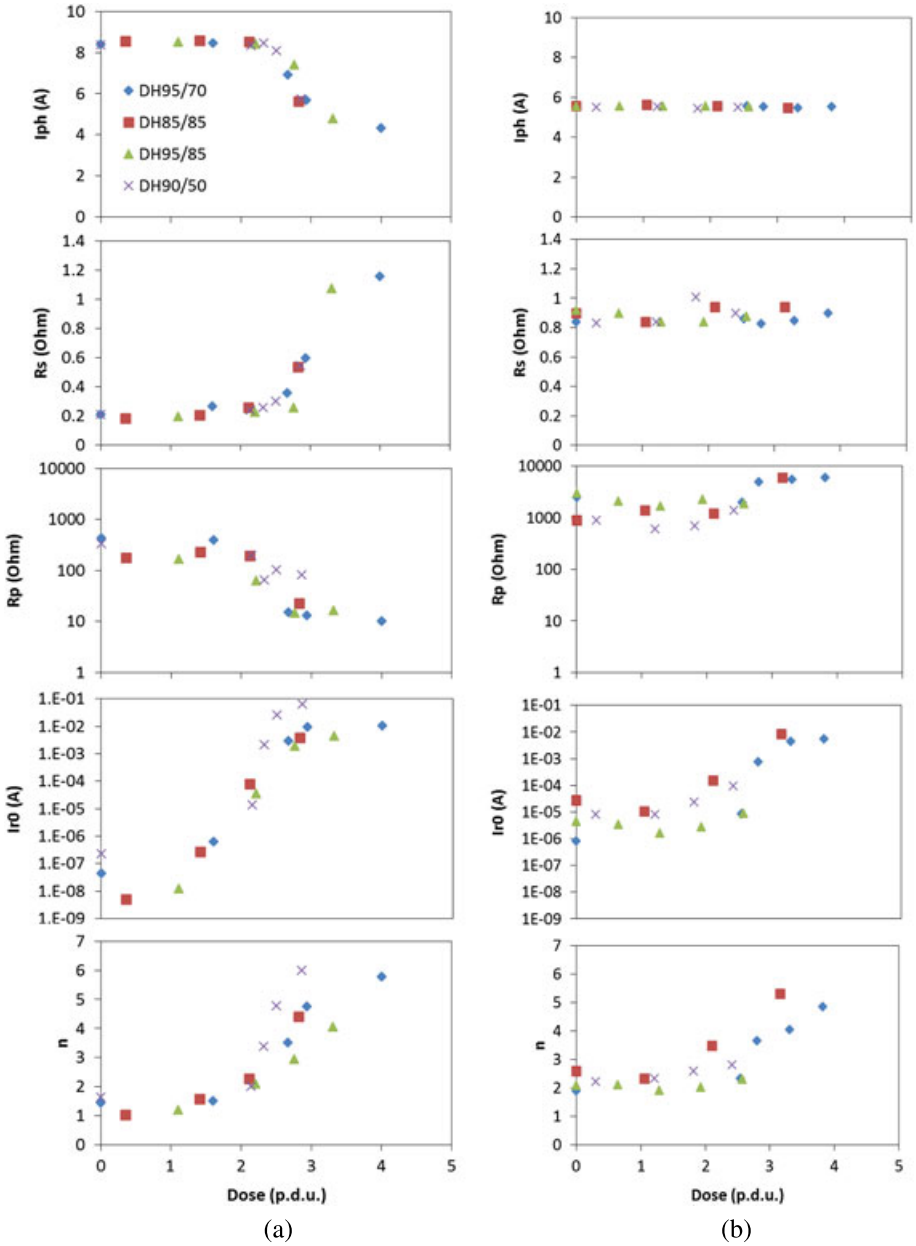

Figure 8. Degradations of photocurrent (I_{ph}), series resistance (R_s), parallel resistance (R_p), diode recombination current (I_{r0}) and diode ideality factor (n) against humidity dose in dependence of damp-heat conditions for (a) Module Type A and (b) Module Type B.

inhomogeneous degradation can be supported by the EL images as the cells in a module had different brightness and the difference in brightness became more significant while modules were degrading (as shown in Figure 3b). This may be due to the modules having a stronger moisture barrier in their backsheet and the water vapour could mainly come into module from the module periphery and junction box area, which caused inhomogeneous degradations. To summarise, the B type modules had a very different degradation mode, which is due to the module's inhomogeneous ageing and slightly increasing cell mismatch.

4. CONCLUSIONS

A number of extended DH tests at different temperature and RH levels have been carried out within the SOPHIA project. Three types of PV modules with different cells, encapsulants and backsheets were used for the accelerated ageing tests. Different types of module saw different degradation phenomena because of its design, manufacturing process and materials used. Modules of the same type exhibited the same degradation behaviours in I-V curves and solar cell equivalent circuit parameters, although they were aged under different DH conditions. This indicates

DOI: 10.1002/pip

that all modules of a given type experienced the same ageing modes independent of the various DH stresses.

The module Type A with the EVA encapsulant and polymer backsheet suffered significantly by DH exposure. Its degradation in power was mainly attributed to the losses in I_{ph} and R_s because of the water ingress into module that caused corrosions of electrical circuits and damages of cell finger bonding. The module Type B has an aluminium barrier embedded in its backsheet, which greatly minimised the rate of moisture permeation from backsheet. Although the whole ageing process of the B type modules was not observed before the end of the tests, the main contributor to the power degradation appeared to be the mismatch in cells as each cell degraded at different degradation rates. The module Type C with the thermoplastic material as encapsulant showed minor degradation due to DH stress, except for the modules aged at 95°C that saw early failures due to the melting of thermoplastic encapsulant.

The aformentioned degradation mechanisms of Type A and Type B modules were identified by analysing the degradations of device power as well as the changes of solar cell equivalent circuit parameters against the derived humidity dose. By using this approach, the different driven factor for the device's power degradation can be identified at different stages of the ageing process. The analysis can be applied to modules undergone different ageing processes indoors or outdoors. This allows further investigations of the device ageing mechanisms and assists the development of new appropriate accelerated stress tests.

ACKNOWLEDGEMENTS

This work was supported in part by the European Commission under FP7 grant N° 262533 SOPHIA (INFRA-2010-1.1.22_CP-CSA-Infra) and by the Research Councils UK (RCUK) under project 'Stability and Performance of Photovoltaics (STAPP)' (contract no: EP/H040331/1).

REFERENCES

1. Osterwald CR, McMahon TJ. History of accelerated and qualification testing of terrestrial photovoltaic modules: a literature review. *Progress in Photovoltaics: Research and Applications* 2009; **17**: 11–33.
2. Bennett IJ, Zhu J, Gottschalg R, Köhl M, Hoffmann S, Berger KA, Zamini S, Gerritsen E, Malbranche P, Pugliatti PM, Di Stefano A, Aleo F, Bertani D, Paletta F, Roca F, Graditi G, Pellegrino M, Zubillaga O, Cano P, PV module lifetime prediction and quality assurance as addressed by Sophia, in *Proc. 29th EU PVSEC*, 2014, pp. 2495–2498.
3. Zhu J, Gottschalg R, Koehl M, Hoffmann S, Berger KA, Zamini S, Bennett IJ, Gerritsen E, Malbranche P, Pugliatti P, Di Stefano A, Aleo F, Bertani D, Paletta F, Roca F, Graditi G, Pellegrino M, Zubillaga O, Cano P, Pozza A, Sample T, Changes of solar cell parameters during dampheat exposure, in *Tech. Dig. WCPEC 6*, 2014.
4. Berger KA, Kubicek B, Ujvari G, Leidl R, Krametz T, Zamini S, Hoffmann S, Koehl M, Pozza A, Sample T, Bertani D, Paletta F, Bennett IJ, Gerritsen E, Malbranche P, Zhu J, Gottschalg R, Pugliatti P, Di Stefano A, Aleo F, Roca F, Graditi G, Pellegrino M, Zubillaga O, Cano P, Investigation of thermo-mechanical stresses on PV Modules: a collaborative research within the European Photovoltaic Infrastructure Research Project SOPHIA, in *Tech. Dig. WCPEC 6*, 2014.
5. Malbranche P, Merten J, Assoa B, Gerritsen E, Bergeron F, Albaric M, Varache R, Cros S, Siefer G, Koehl M, Schubert M, Warta W, Misara S, Sprenger W, Pozza A, Taylor N, Sample T, Paletta F, Bennett IJ, Kroon J, Zhu J, Gottschalg R, Zamini S, Berger KA, Pugliatti P, Di Stefano A, Aleo F, Roca F, Graditi G, Pellegrino M, Zubillaga O, Cano P, Gordon I, Gevorgyan S, Lauermann I, Hinrichs V, Schmid M, Huepkes J, Augarten Y, Anton I, Rousu S, Hast J, Pettersen T, Juel M, Basso P, Arrowsmith G, Valente V, Craciun D, Optimising PV research infrastructures in Europe: lessons learned from the SOPHIA Project, in *Tech. Dig. WCPEC 6*, 2014.
6. IEC 61215 Ed. 2. *Crystalline Silicon Terrestrial Photovoltaic (PV) Modules—Design Qualification and Type Approval*. IEC Central Office: Geneva, Switzerland, 2005.
7. Wohlgemuth JH, Kempe MD, Equating damp heat testing with field failures of PV modules, in *Proc. 39th IEEE PVSC*, 2013, pp. 126–131.
8. Wohlgemuth JH, Kurtz S, Using accelerated testing to predict module reliability, in *Proc. 37th IEEE PVSC*, 2011, pp. 3601–3605.
9. Wohlgemuth JH, Cunningham DW, Amin D, Shaner J, Xia Z, Miller J, Using accelerated tests and field data to predict module reliability and lifetime, in *Proc. 23rd EUPVSEC*, 2008, pp. 2663–2669.
10. Wohlgemuth JH, Cunningham DW, Nguyen AM, Miller J, Long term reliability of PV modules, in *Proc. 20th EUPVSEC,* 2005, pp. 1942–1946.
11. Hacke P, Terwilliger K, Glick S, Trudell D, Bosco N, Johnston S, Kurtz S, Test-to-Failure of crystalline silicon modules, in *Proc. 35th IEEE PVSC*, 2010, pp. 244–250.
12. Quintana MA, King DL, McMahon TJ, Osterwald CR, Commonly observed degradation in field-aged photovoltaic modules, in *Proc. 29th IEEE PVSC*, 2002, pp. 1436–1439.
13. Jorgesen GJ, Terwilliger KM, Del Cueto JA, Glick SH, Kempe MD, Pankow JW, Pern FJ, McMahon TJ. Moisture transport, adhesion and corrosion

DOI: 10.1002/pip

protection of PV module packing materials. *Solar Energy Materials and Solar Cells* 2006; **90**: 2739–2775.
14. Voronko Y, Eder GC, Knausz M, Oreski G, Koch T, Berger KA. Correlation of the loss in photovoltaic module performance with the ageing behaviour of the backsheets used. *Progress in Photovoltaics: Research and Applications* 2015; **23**: 1501–1515.
15. Masuda A, Suzuki S, Hara Y, Sakamoto S, Doi T, Possible measure of reliability for Crystalline-Si photovoltaic modules, in *Proc. 29th EUPVSEC*, 2014, pp. 2566–2569.
16. Czanderna AW. Encapsulation of PV modules using ethylene vinyl acetate copolymer as a pottant: a critical review. *Solar Energy Materials and Solar Cells* 1996; **43**(2): 101–181.
17. Ketola B, Norris A, Degradation mechanism investigation of extended damp heat aged PV modules, in *Proc. 26th EUPVSEC,* 2011.
18. Kempe MD, Jorgensen GJ, Terwilliger KM, McMahon TJ, Kennedy CE, Borek TT. Acetic acid production and glass transition concerns with ethylene-vinyl acetate used in photovoltaic devices. *Solar Energy Materials and Solar Cells* 2007; **91**: 315–329.
19. Marín ML, Jiménez A, López J, Vilaplana J. Thermal degradation of ethylene (vinyl acetate) – kinetic analysis of thermogravimetric data. *Journal of Thermal Analysis* 1996; **47**(1): 247–258.
20. Sakamoto S, Shimizu S, Kadowaki M, Tanaka H, Suzuki K, Gobou K, Yamamoto C, Doi T, Masuda A, Comparison of degradation mechanism of PV Modules between under long term field exposure at hot-humid environment and under DH tests, in *Proc. 29th EUPVSEC*, 2014, pp. 3364–3367.
21. Jordan DC, Kurtz SR. Photovoltaic degradation rates —an analytical review. *Progress in Photovoltaics: Research and Applications* 2013; **21**: 12–29.
22. Wu D, Zhu J, Betts TR, Gottschalg R. Degradation of interfacial adhesion strength within photovoltaic mini-modules during damp-heat exposure. *Progress in Photovoltaics: Research and Applications* 2014; **22**: 796–809.
23. Benoît Braisaz, Chloé Duchayne, Mike Van Iseghem, Khalid Radouane, PV ageing model applied to several metrological condition, in *Proc. 29th EUPVSEC*, 2014, pp. 2303–2309.
24. Meyer EL, van Dyk EE. Assessing the reliability and degradation of photovoltaic module performance parameters. *IEEE Transactions on Reliability* 2004; **53**(1): 83–92.
25. Gottschalg R, Betts TR, Eeles A, Williams SR, Zhu J. Influences on the energy delivery of thin film modules. *Solar Energy Materials and Solar Cells* 2013; **119**: 169–180.
26. B. Mihaylov, J.W. Bowers, T.R. Betts, R. Gottschalg, T. Krametz, R. Leidl, K.A. Berger, S. Zamini, N.J.J. Dekker, G. Graditi, F. Roca, M. Pellegrino, G. Flaminio, G. Razongles, J. Merten, A. Pozza, E. Salis, R.P. Kenny, G. Friesen, S. Dittmann, Results of the SOPHIA Module Intercomparison Part-2: STC, low irradiance conditions and temperature coefficients measurements of thin film technologies, in *Proc. 31st EU PVSEC*, 2015.
27. Herrmann W, Bogdanski N, Outdoor weathering of PV modules - effects of various climates and comparison with accelerated laboratory testing, in *Proc. 37th IEEE PVSC,* 2011, pp. 2305–2311.
28. Eades WD, Swanson RM. Calculation of surface generation and recombination velocities at the Si-SiO2 interface. *Journal of Applied Physics* 1985; **58**: 4267.
29. Wu X, Bliss M, Sinha A, Betts TR, Gupta R, Gottschalg R. Accelerated spatially resolved electrical simulation of photovoltaic devices using photovoltaic-oriented nodal analysis. *IEEE Transactions on Electron Devices* 2015; **62**(5): 1390–1398.
30. Monokroussos, C., et al, Effect of cell width on the device performance of amorphous silicon solar cells, in *Proc. 19th EU PVSEC*, 2004.
31. Kempe, M.D., Control of moisture ingress into photovoltaic modules, in *Proc. 31st IEEE PVSC*, 2005, pp. 503–506.
32. Koehl M, Heck M, Wiesmeier S. Modelling of conditions for accelerated lifetime testing of Humidity impact on PV-modules based on monitoring of climatic data. *Solar Energy Materials and Solar Cells* 2012; **99**: 282–291.
33. Buehler AJ, Krenzinger A. Method for photovoltaic parameter extraction according to a modified double-diode model. *Progress in Photovoltaics: Research and Applications* 2012; **21**: 884–893.
34. Chan DSH, Phang JCH. Analytical methods for the extraction of solar-cell single and double diode model parameters from I–V characteristics. *IEEE Transactions on Electron Devices* 1987; **34**(2): 286–293.
35. Garrido-Alzar CL. Algorithm for extraction of solar cell parameters from I–V curve using double exponential model. *Renewable Energy* 1997; **10**(2/3): 125–128.
36. Sandrolini L, Artioli M, Reggiani U. Numerical method for the extraction of photovoltaic module double-diode model parameters through cluster analysis. *Applied Energy* 2010; **87**: 442–451.
37. Nishioka K, Sakitani N, Uraoka Y, Fuyuki T. Analysis of multicrystalline silicon solar cells by modified

DOI: 10.1002/pip

3-diode equivalent circuit model taking leakage current through periphery into consideration. *Solar Energy Materials and Solar Cells* 2007; **91**: 1222–1227.
38. Gottschalg R, Rommel M, Infield DG, Kearney MJ, Ryssel H. Influence of the measurement environment on the extraction of the physical parameters of solar cells. *Measurement Science and Technology* 1999; **9**: 794–803.
39. Peike C, Hoffmann S, Hulsmann P, Thaidigsmann B, Weiss KA, Koehl M, Bentz P. Origin of damp-heat induced cell degradation. *Solar Energy Materials and Solar Cells* 2013; **116**: 49–54.

 2016; **24**:1346–1358
DOI: 10.1002/pip